Supplementary Data

Npl3 functions in mRNP assembly by recruitment of mRNP components to the transcription site and their transfer onto the mRNA

Philipp Keil, Alexander Wulf, Nitin Kachariya, Samira Reuscher, Kristin Hühn, Ivan Silbern, Janine Altmüller, Ralf Stehle, Kathi Zarnack, Michael Sattler, Henning Urlaub and Katja Sträßer

Design of Npl3 mutants with impaired RNA-binding activity

In order to obtain Npl3 mutants with reduced RNA-binding activity, we mutated amino acids in the RNA recognition motif 1 (RRM1), linker and RRM2 domains of Npl3 that cross-linked to RNA *in vivo* (Supplementary Table S1 and Supplementary Figure S1A). For RRM1 we tested single, double and triple mutations of the three conserved phenylalanines (F) to tyrosine (Y) in the RNP1 motif (F160, F162 and F165; Supplementary Figure S1A). All mutant npl3 proteins are expressed at wild-type (wt) levels *in vivo* (Supplementary Figure S1B). Since mutation of F162 is sufficient for the observed growth defect and the temperature sensitive phenotype (ts and cs, Supplementary Figure S1C), we chose this mutant for further analysis. In the linker region we mutated proline (P) 196 and alanine (A) 197 to aspartic acid (D). In RRM2, we mutated F245 in RNP2 to a Y or an inosine (I). Both mutant proteins are expressed at wt levels *in vivo* (Supplementary Figure S1D) and cause a temperature sensitive growth phenotype (Supplementary Figure S1E). As *npl3-F245I* cells grow a bit better at 30°C than *npl3-F245Y* cells (Supplementary Figures S1E, S2E), we chose the former for further analysis.

NMR spectroscopy and structural analysis

Structural modeling. We characterized the overall conformation and internal flexibility of the $Npl3^{120-280}$ protein using solution nuclear magnetic resonance (NMR) spectroscopy. The overall tumbling correlation time (Supplementary Figure S3C) derived from NMR ^{15}N relaxation experiments indicates that the two domains are arranged in a rather fixed orientation and do not reorient independently. The data also show that the N-terminal tail and the C-terminal tail regions flanking the two RRM domains are flexible (Supplementary Figure S3B-E). Interestingly, heteronuclear nuclear Overhauser effect (NOE) data (Supplementary Figure S3D) demonstrate that the linker connecting the two RRM domains has only reduced flexibility. The structural arrangement of the Npl3 tandem domains was then defined by inter-domain distance restraints derived from paramagnetic relaxation enhancement (PRE) experiments following our previously reported approach in a semi-rigid body structure calculation (see methods) (1) (Figure 3C, Supplementary Figure S5A-E). The calculated tandem RRM structure of Npl3 is in good agreement with experimental PRE and small angle X-ray scattering (SAXS) data (Supplementary Figure S5D). The structural model (Figure 3C) shows that the RNA-binding surfaces of the two RRM domains face towards each other, forming a positively charged surface (Figure 3D).

Npl3 RRM1 and RRM2 binding preference. We assessed the RNA-binding specificity of Npl3 RRM1 and RRM2 using NMR titrations with short single-stranded DNA oligos. It has been shown before that ssDNA ligands can well represent the RNA recognition by RRMs (2), especially in the case of SRSF1. The maximum NMR chemical shift perturbation observed with the RNP1 and RNP2 binding sites for RRM1 and within the non-canonical conserved motif in RRM2 is plotted in Figure 3B and Supplementary Figure S4A-F, for the oligo sequences indicated.

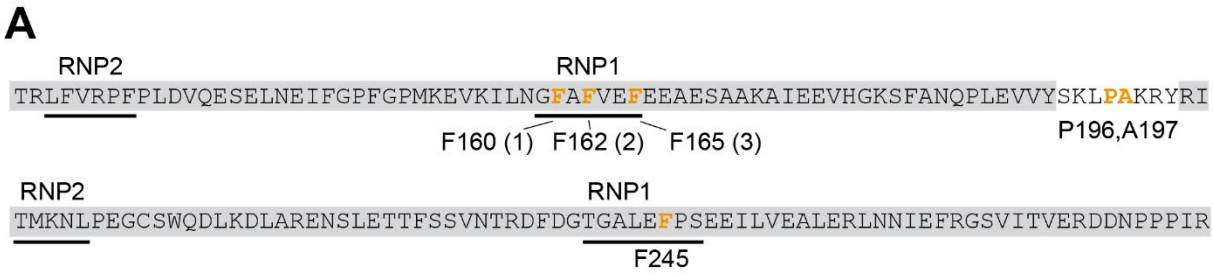
A
RNP2
RNP1
TRLFVRPFPLDVQESELNEIFGPFGPMKEVKILNGFAFVEFEEAESAAKAIEEVHGKSFANQPLEVVYSKLPAKRYRI
F160 (1)
F162 (2)
F165 (3)
P196,A197
RNP2
RNP1
TMKNLPEGCSWQDLKDLARENSLETTFSSVNTRDFDGTGALEFPSEEILVEALERLNNIEFRGSVITVERDDNPPPIR
F245

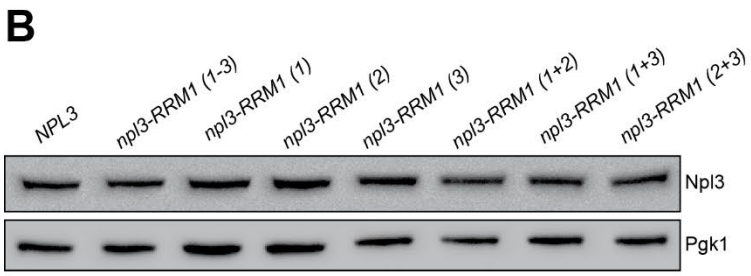
B
NPL3
npl3-RRM1 (1-3)
npl3-RRM1 (1)
npl3-RRM1 (2)
npl3-RRM1 (3)
npl3-RRM1 (1+2)
npl3-RRM1 (1+3)
npl3-RRM1 (2+3)
Npl3
Pgk1

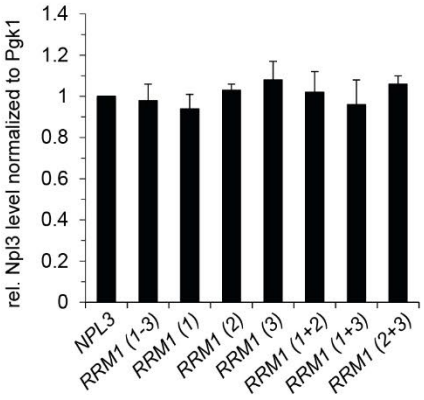
rel. Npl3 level normalized to Pgk1
1.4
1.2
1
0.8
0.6
0.4
0.2
0
NPL3
RRM1 (1-3)
RRM1 (1)
RRM1 (2)
RRM1 (3)
RRM1 (1+2)
RRM1 (1+3)
RRM1 (2+3)

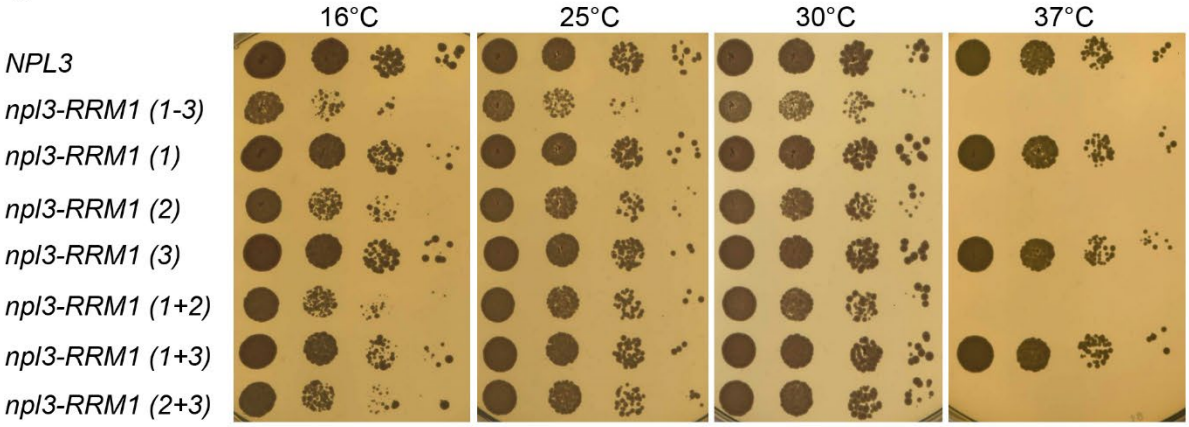
C
16°C
25°C
30°C
37°C
NPL3
npl3-RRM1 (1-3)
npl3-RRM1 (1)
npl3-RRM1 (2)
npl3-RRM1 (3)
npl3-RRM1 (1+2)
npl3-RRM1 (1+3)
npl3-RRM1 (2+3)

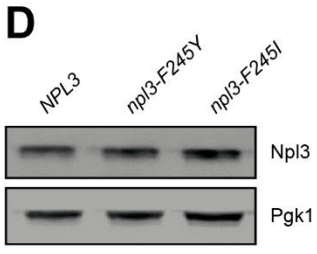
D
NPL3
npl3-F245Y
npl3-F245I
Npl3
Pgk1

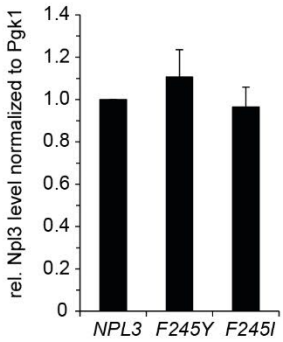
rel. Npl3 level normalized to Pgk1
1.4
1.2
1.0
0.8
0.6
0.4
0.2
0
NPL3
F245Y
F245I

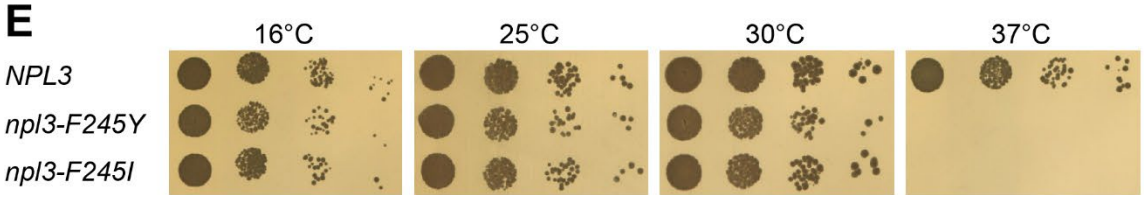
E
16°C
25°C
30°C
37°C
NPL3
npl3-F245Y
npl3-F245I

Supplementary Figure S1. Analysis of mutations in the RRM1 and RRM2 domains of Npl3. (**A**) Scheme of the RRM1-Linker-RRM2 region of Npl3 indicating the RNA-cross-linked amino acids of and mutations in Npl3. For the *npl3-RRM1* mutant F162 was mutated to tyrosine (Y), for *npl3-Linker* P196 and A197 were mutated to aspartic acid (D) and for *npl3-RRM2* F245 was mutated to isoleucine (I).
(**B**) Npl3 variants with mutations in the RRM1 domain are expressed at wt levels *in vivo*. Total Npl3 protein levels were determined by Western blot of whole-cell extracts from *NPL3* cells and cells expressing versions of Npl3 with the first (1), second (2) or third (3) phenylalanine mutated or combinations thereof. Left panel: Western blots, right panel: Quantification of three independent experiments. (**C**) Mutation of F162 to Y in the RRM1 of Npl3 is sufficient for the observed growth phenotype. F160, F162 and/or F165 (3) were mutated to Y either all three simultaneously (1-3), combinations of two mutations (1+2, 1+3 and 2+3) or the separately (1, 2 and 3). Mutation of F162 (2) confers the temperature sensitive phenotype.10-fold serial dilutions of wt cells and the indicated *npl3-RRM1* mutants were spotted onto YPD plates and grown for 2-3 days at the indicated temperatures. (**D**) Npl3 variant with mutations in the RRM2 domain of Npl3 are expressed at wt levels *in vivo*. Determination of total protein levels of npl3-F245Y and F245I mutants as in B. (**E**) Mutation of F245 to Y or I in the RRM2 of Npl3 causes a growth phenotype. Experiment as in C.

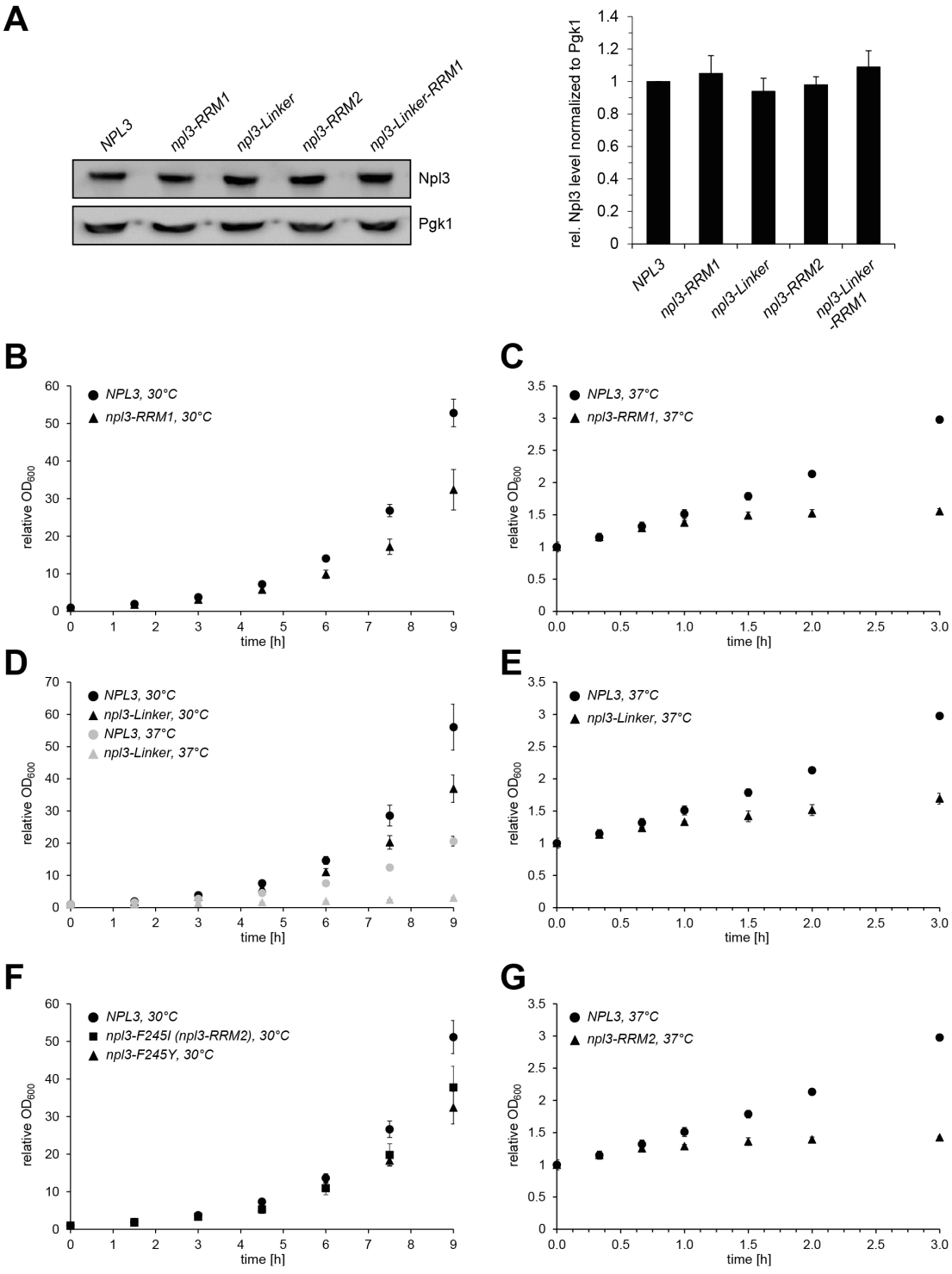

Supplementary Figure S2. Expression levels and growth curves of the three *npl3* mutants *npl3-RRM1*, *-Linker* and *-RRM2*. (**A**) Npl3 variant with mutations in the RRM1-, linker- and RRM2-domains of Npl3 are expressed at wt levels *in vivo*. Experiment as in Supplementary Figure S1B. (**B - G**) Growth curves of the *npl3-RRM1*, *-Linker* and *-RRM2* mutant at 30°C and 37°C as indicated.

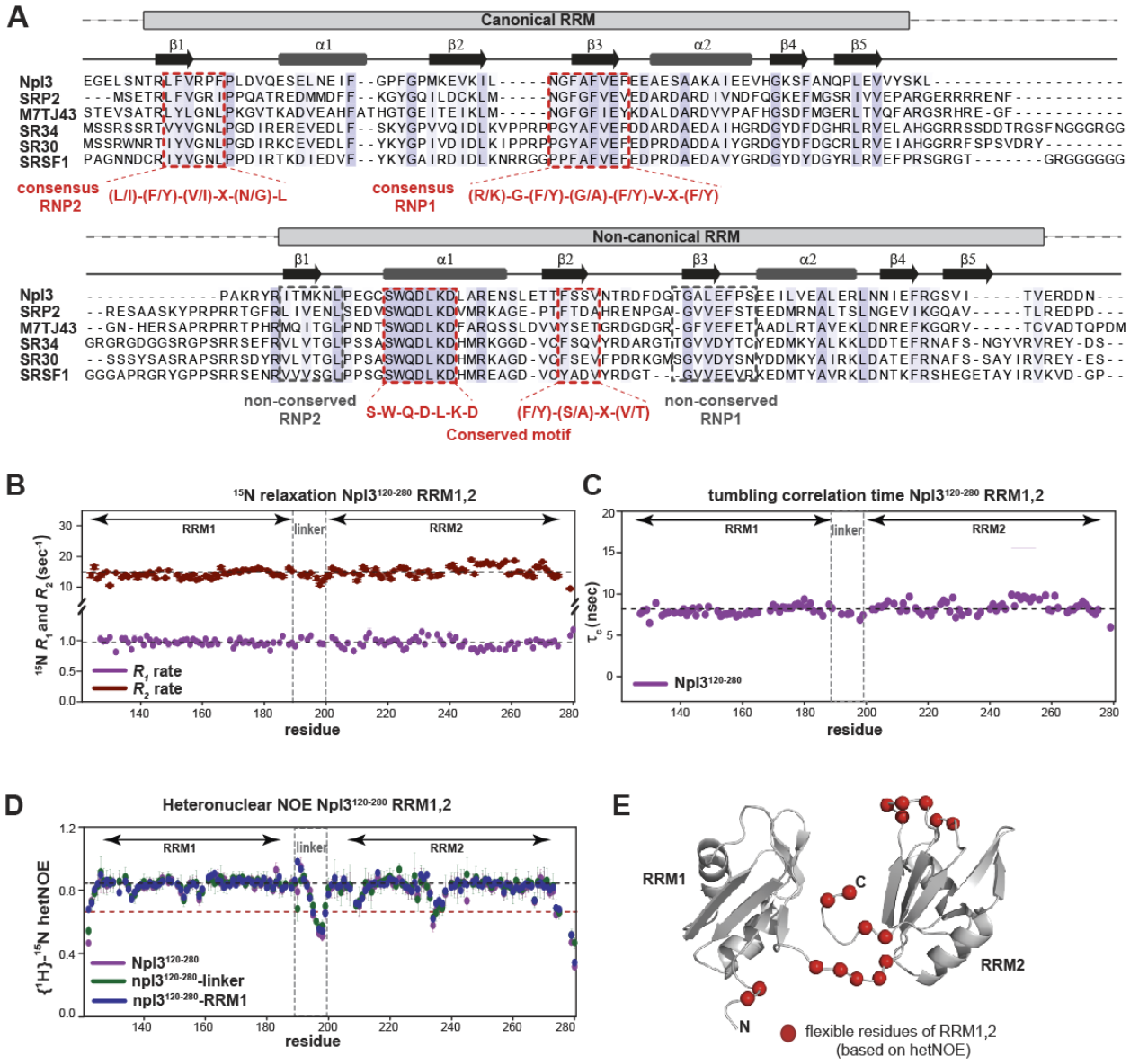

Supplementary Figure S3. Sequence conservation and NMR characterization of Npl3 RRM1,2. (**A**) Multiple sequence alignment of RRM domains from SR-like proteins across the various species using Clustal omega (https://www.ebi.ac.uk/Tools/msa/clustalo/) and Jalview (https://www.jalview.org/) tools. The red dashed line highlights the alignment of consensus RNP motifs in RRM1 and the non-canonical binding region in RRM2. (**B**) NMR ^{15}N longitudinal (R_1) and transverse (R_2) relaxation rates at 900 MHz proton Larmor frequency. Average R_1 and R_2 rates are 0.97 sec^{-1} and 14.8 sec^{-1}, respectively. (**C**) Residue-specific correlation times (τ_c) calculated from R_1 and R_2 rates. The average correlation time is 8.1 ns. (**D**) Comparison of {^{1}H}-^{15}N heteronuclear NOE of wildtype and mutants of RRM1,2. Linker between RRM domains shown with gray box. (**E**) Residues with fast scale dynamics are highlighted on structure with red spheres.

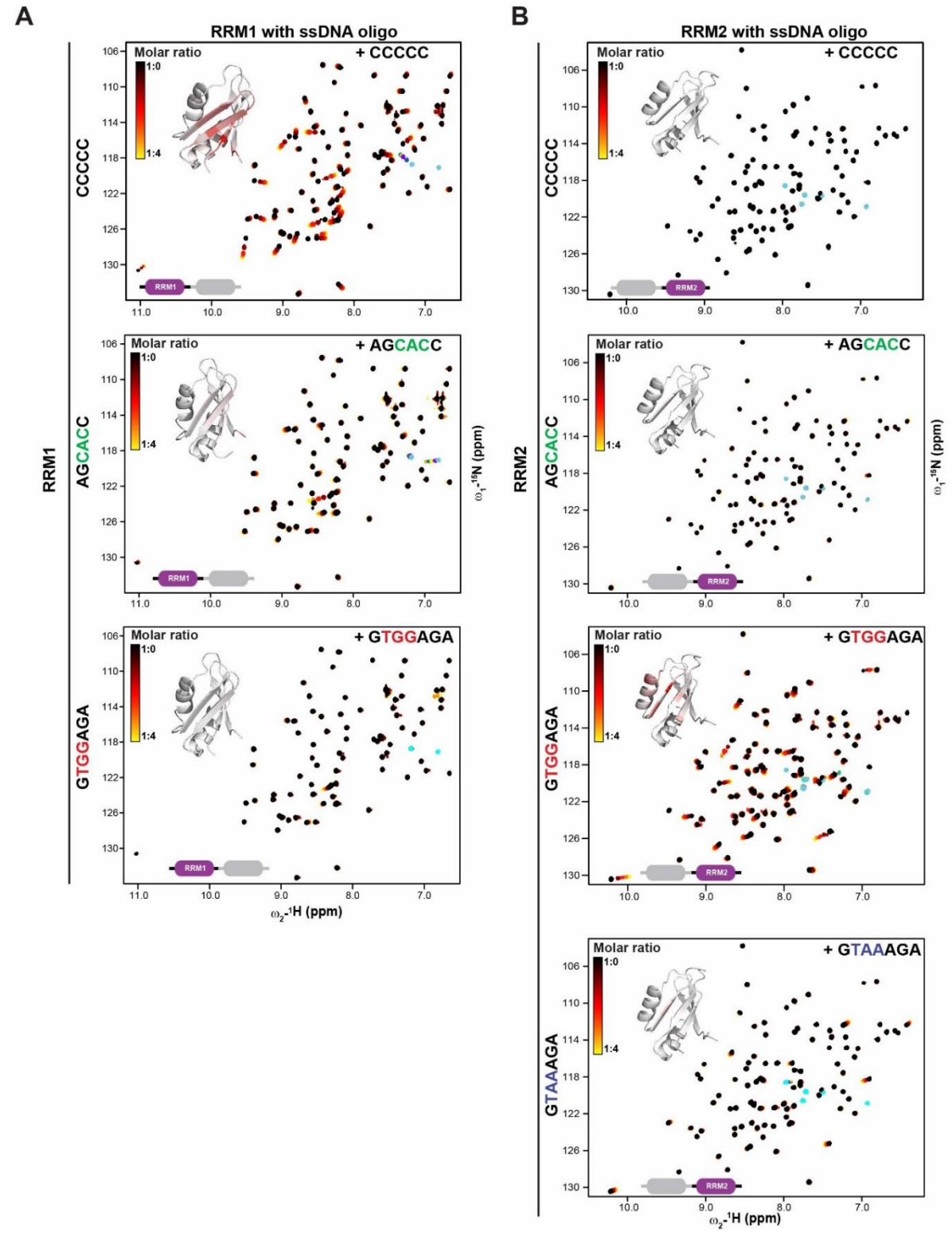
A
RRM1 with ssDNA oligo
RRM1
CCCCC
AGCACC
GTGGAGA
Molar ratio
1:0
1:4
+ CCCCC
+ AGCACC
+ GTGGAGA
RRM1
ω_1-^{15}N (ppm)
ω_2-^{1}H (ppm)
B
RRM2 with ssDNA oligo
RRM2
CCCCC
AGCACC
GTGGAGA
GTAAAGA
Molar ratio
1:0
1:4
+ CCCCC
+ AGCACC
+ GTGGAGA
+ GTAAAGA
RRM2
ω_1-^{15}N (ppm)
ω_2-^{1}H (ppm)

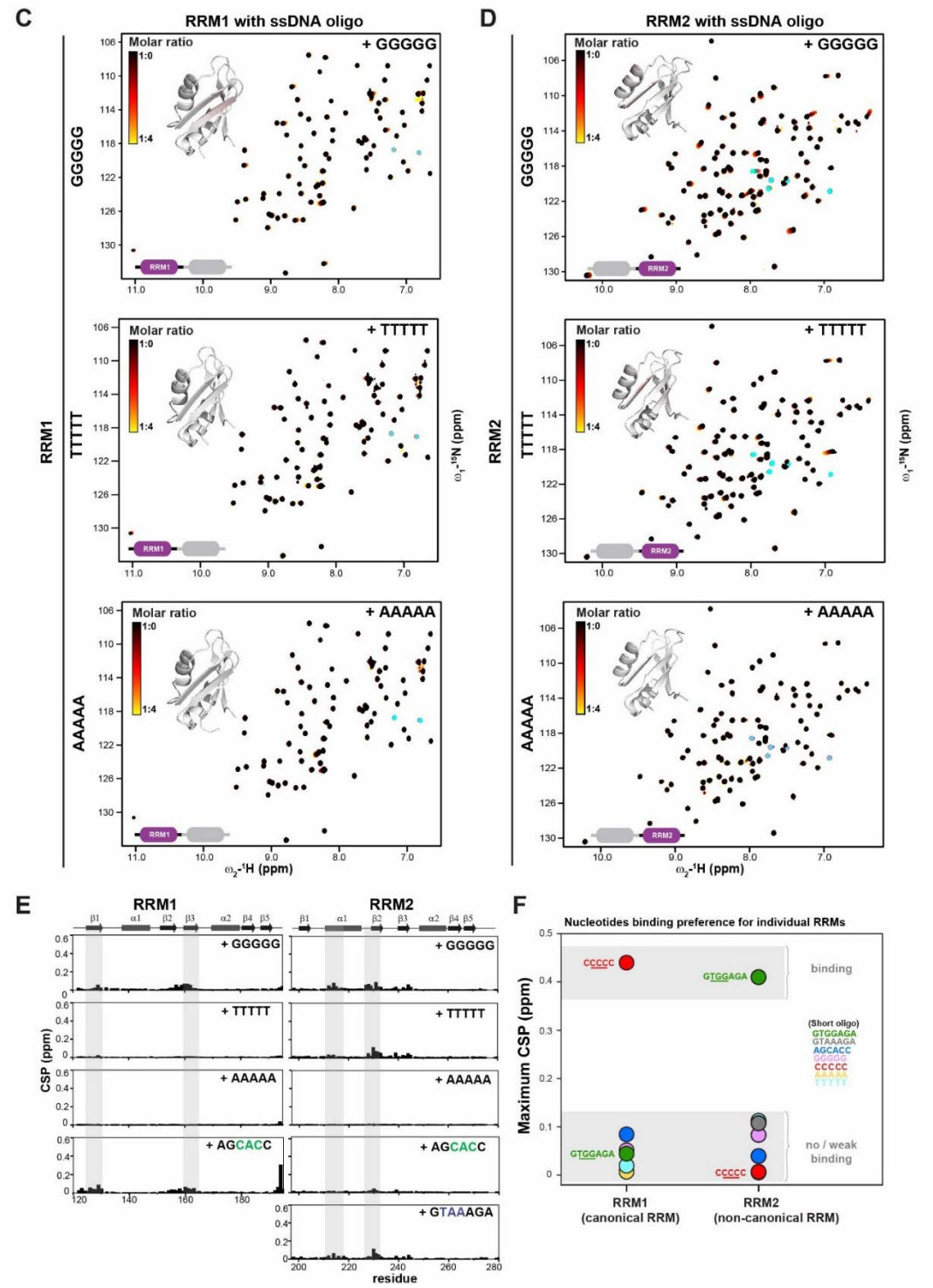

Supplementary Figure S4. NMR titrations to assess the RNA-binding preference of Npl3. Superposition of NMR ^{1}H-^{15}N correlation spectra of (**A,C**) RRM1 (left) and (**B,D**) RRM2 (right) titrated with various single-stranded DNA oligonucleotides. Spectra are colored black (free) and red to yellow (with increasing ligand concentration). Chemical shift perturbations (CSP) are mapped (red) onto the structure of the RRM domains. (**E**) Summary of the CSPs. RNP1, RNP2 and non-canonical conserved sites are highlighted with gray boxes. (**F**) Binding preferences for RRM1 (left) and RRM2 (right) based on maximum CSPs.

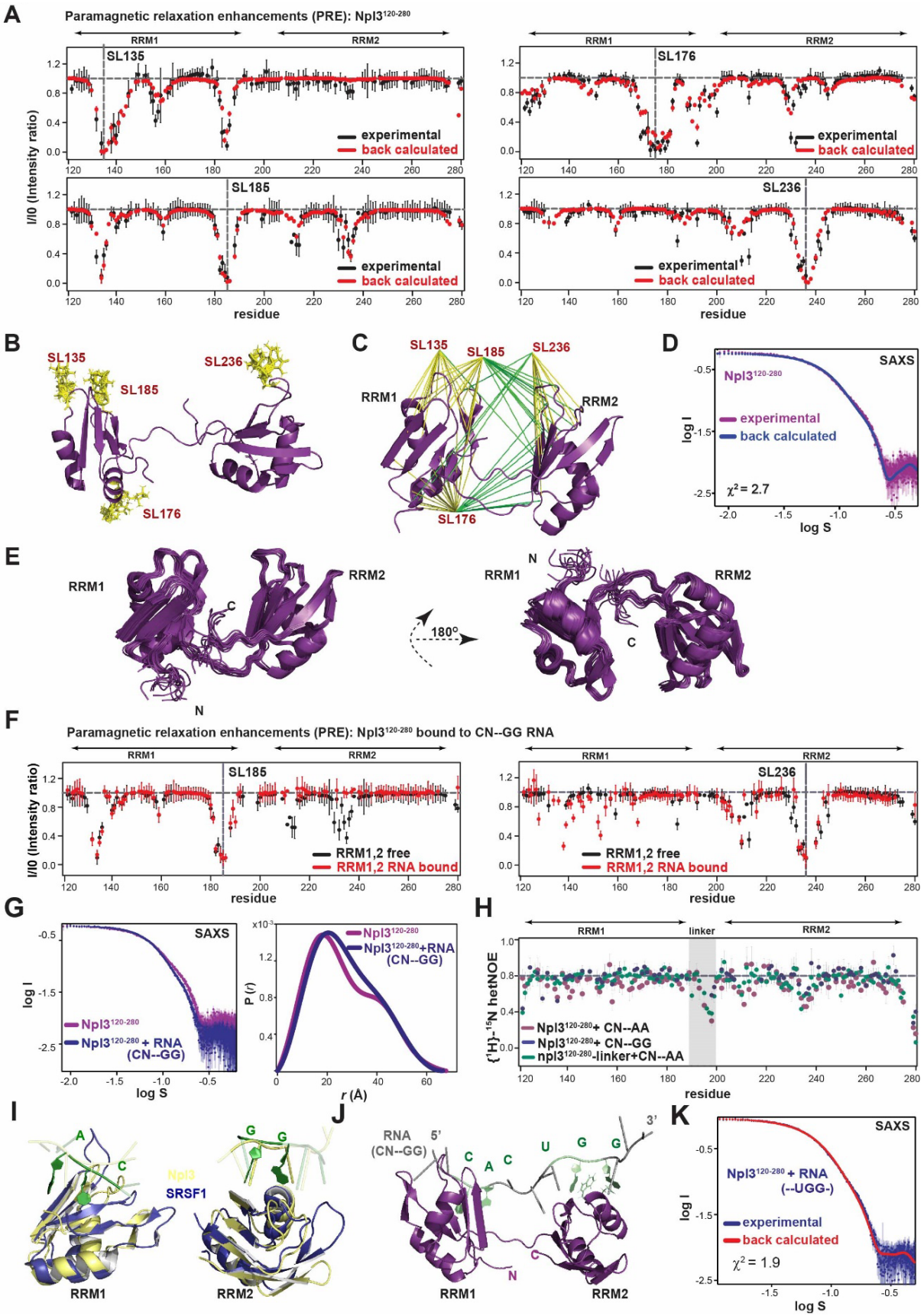
A
Paramagnetic relaxation enhancements (PRE): Npl3120-280
RRM1
RRM2
SL135
SL176
SL185
SL236
experimental
back calculated
I/I0 (Intensity ratio)
residue
B
C
D
SAXS
log I
log S
χ2 = 2.7
E
180°
N
C
F
Paramagnetic relaxation enhancements (PRE): Npl3120-280 bound to CN--GG RNA
RRM1,2 free
RRM1,2 RNA bound
G
Npl3120-280
Npl3120-280 + RNA (CN--GG)
P (r)
r (Å)
H
linker
{1H}-15N hetNOE
Npl3120-280+ CN--AA
Npl3120-280+ CN--GG
npl3120-280-linker+CN--AA
I
Npl3
SRSF1
J
RNA (CN--GG)
5'
3'
K
Npl3120-280 + RNA (--UGG-)
χ2 = 1.9

Supplementary Figure S5. Structure of the Npl3 RRM domains free and RNA-bound. (**A**) Paramagnetic relaxation enhancements (PREs) from amide signal intensities in the oxidized and reduced state of spin-labeled protein (black) *vs.* PREs back-calculated from the final model (red). Four positions were spin-labeled individually by introducing mono-Cys variants for residue 135, 176,185 and 236. (**B**) Starting template for structure calculation with an ensemble of four copies for each spin label site indicated by yellow sticks. (**C**) Structural model of Npl3 RRM1,2 based on intra- (yellow lines) and inter-RRM (green lines) distance restraints derived from the experimental PRE data. (**D**) Comparison of experimental small angle X-ray scattering (SAXS) data with those back-calculated from the final structure. (**E**) Superposition of the ensemble of 15 lowest energy structures for the tandem RRM1,2 in two different views. (**F**) PRE data of spin-labeled Npl3 RRM1,2 bound to CN--GG RNA (red) compared to PRE data of the free protein (black) for spin labels at position 185 (RRM1) and 236 (RRM2). (**G**) Experimental SAXS data of free and RNA-bound Npl3 RRM1,2. (**H**) $\{^{1}H\}$-^{15}N heteronuclear NOE of wild-type and linker mutant of RRM1,2 bound to “CN—AA” and “CN—GG” RNA. (**I**) Overlay of the SRSF1 RRM/RNA complex structures (dark blue) with of Npl3 (pale-yellow). CN and GG motifs are colored in green. (**J**) NMR and SAXS-derived structural model of the Npl3 tandem RRM domains with the “CN--GG” RNA. (**K**) Experimental and back calculated SAXS data from RNA-bound model on $Npl3^{120-280}$ are shown. The agreement is indicated by a χ^2 of 1.9.

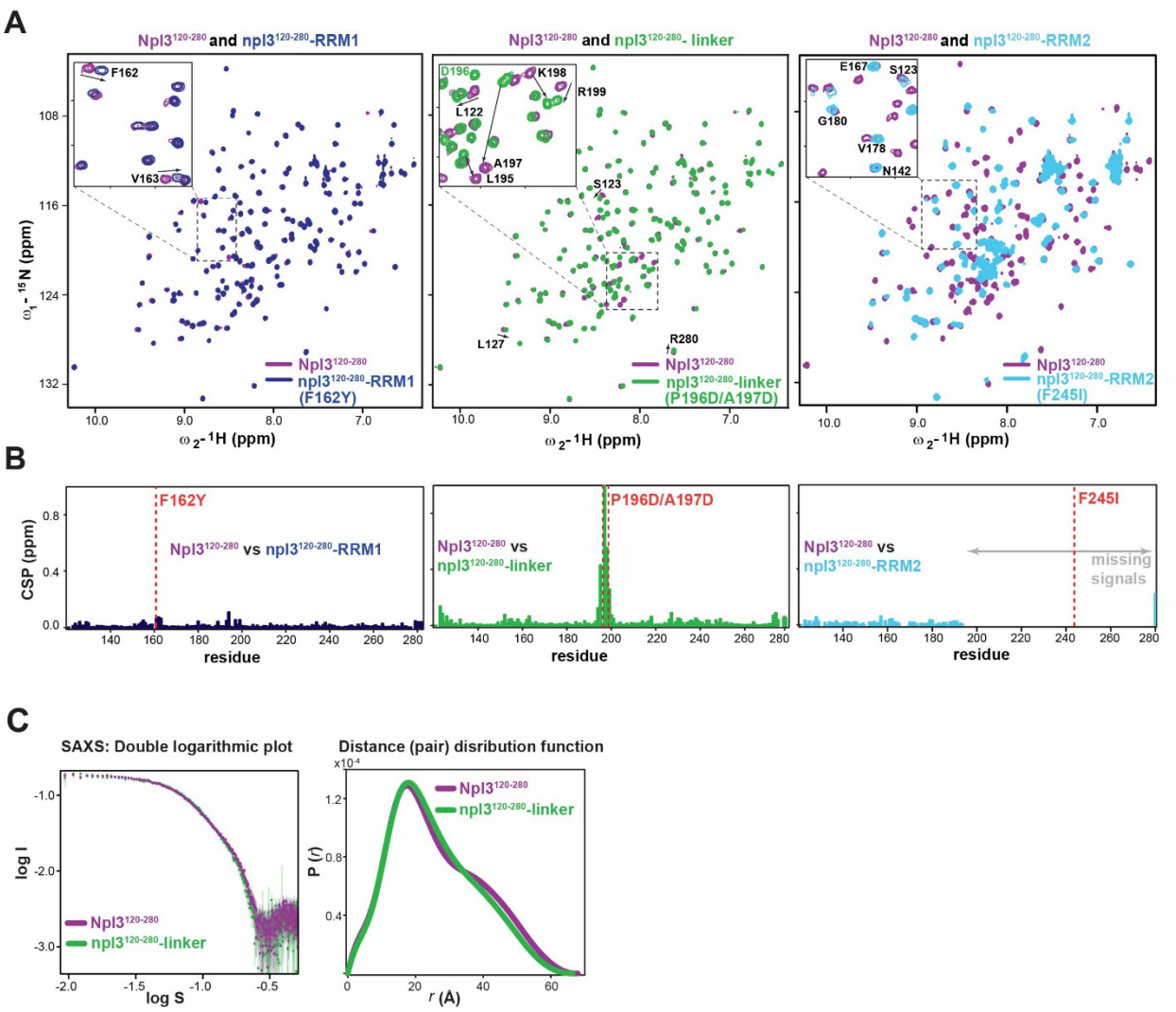

Supplementary Figure S6. Structural effects of mutations on Npl3$^{120-280}$ by NMR and SAXS. (**A**) NMR ^{1}H-^{15}N correlation spectra (HSQC) of wildtype RRM1,2 (purple) superimposed with the RRM1 mutant (dark-blue), linker mutant (green) and RRM2 mutant (cyan), respectively. (**B**) Chemical shift perturbation (CSP) between spectra of wildtype Npl3$^{120-280}$ with npl1-RRM1, npl3$^{120-280}$-linker and npl3$^{120-280}$-RRM2 mutants, respectively. The mutated sites are indicated by red dashed lines. (**C**) SAXS data (left) and distance distribution function *P(r)* (right) for wild-type Npl3$^{120-280}$ and the linker mutant.

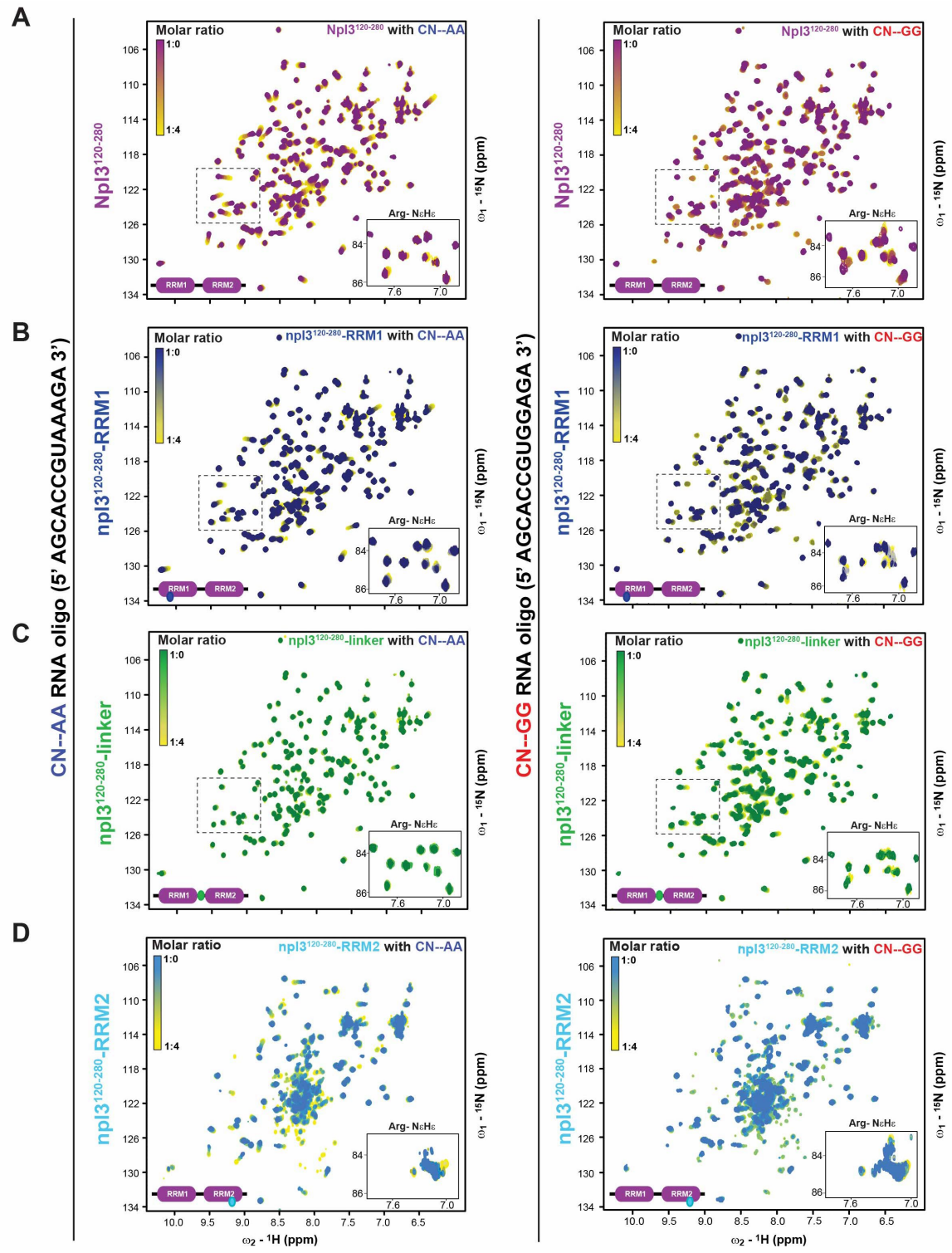

Supplementary Figure S7. RNA binding with wild-type and various mutants of Npl3$^{120-280}$ by NMR. Superposition of NMR ^{1}H-^{15}N correlation spectra of (**A**) ^{15}N labeled wildtype RRM1,2 (purple) (**B**) RRM1 (dark blue), (**C**) Linker –mutant (green) and (**D**) RRM2 (light blue) mutants titrated with "CN--AA" RNA (left) and the "CN--GG" RNA (right). Increasing chemical shift changes are colored from purple, green, dark or light blue (free form) to yellow (RNA-bound form). NMR signals of arginine NεHε side chains are shown as insets.

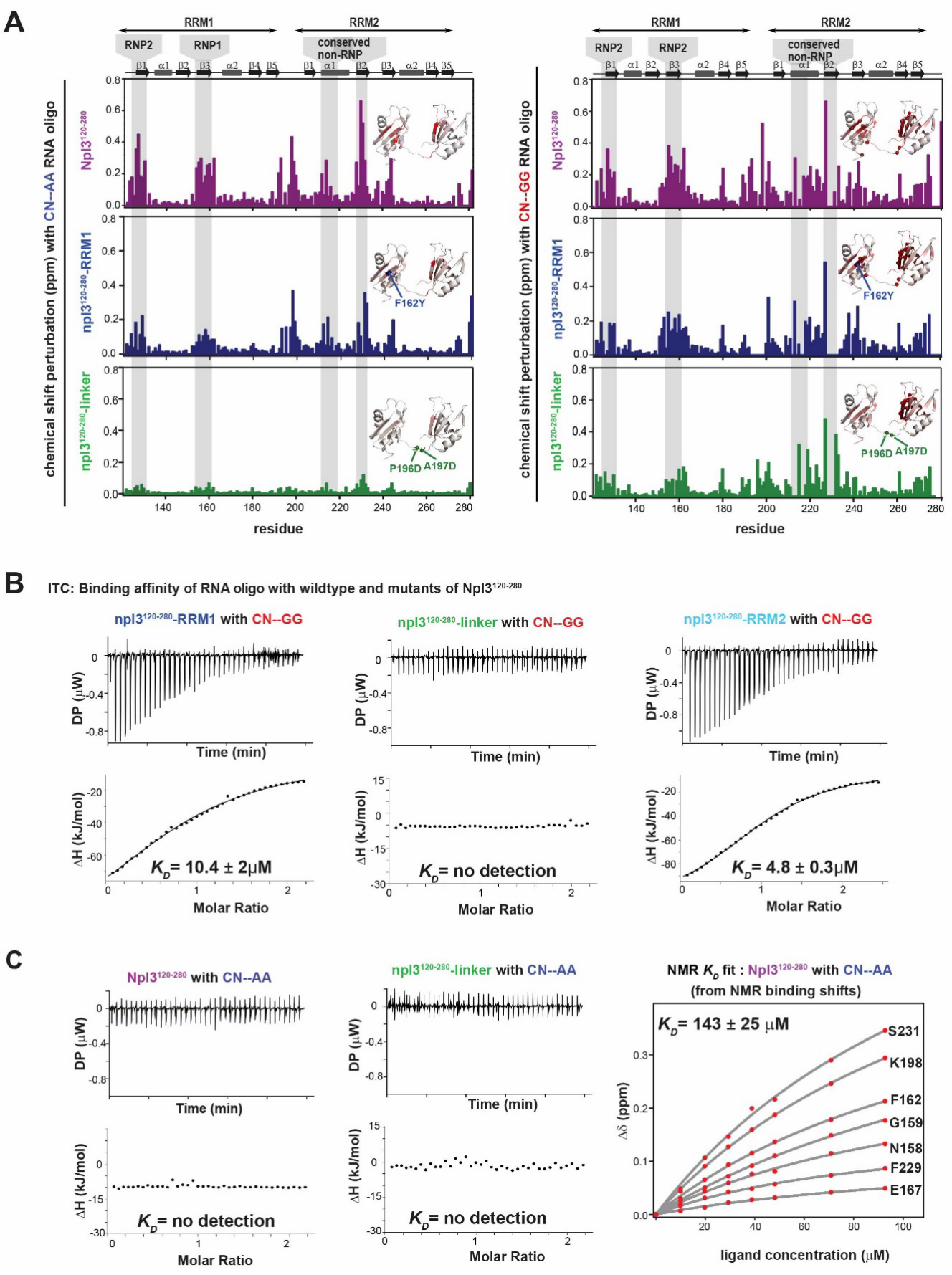
A
RRM1
RRM2
RNP2
RNP1
conserved non-RNP
chemical shift perturbation (ppm) with CN--AA RNA oligo
chemical shift perturbation (ppm) with CN--GG RNA oligo
Npl3120-280
npl3120-280-RRM1
npl3120-280-linker
F162Y
P196D A197D
residue
B
ITC: Binding affinity of RNA oligo with wildtype and mutants of Npl3120-280
npl3120-280-RRM1 with CN--GG
npl3120-280-linker with CN--GG
npl3120-280-RRM2 with CN--GG
DP (μW)
Time (min)
ΔH (kJ/mol)
Molar Ratio
KD= 10.4 ± 2μM
KD= no detection
KD= 4.8 ± 0.3μM
C
Npl3120-280 with CN--AA
npl3120-280-linker with CN--AA
NMR KD fit : Npl3120-280 with CN--AA
(from NMR binding shifts)
KD= 143 ± 25 μM
S231
K198
F162
G159
N158
F229
E167
Δδ (ppm)
ligand concentration (μM)

Supplementary Figure S8. NMR and isothermal titration calorimetry (ITC) analysis of RNA binding to wild-type and mutant Npl3. (**A**) CSP plot for wildtype (purple), npl3-RRM1 (dark blue) and npl3-linker (green) with “CN--AA” (left) and “CN-GG” (right) RNAs from spectra shown in Supplementary Figure S6. Conserved sequence motifs (RNP1, RNP2 in RRM1 and the non-canonical site in RRM2) are highlighted with gray boxes. The inset shows mapping of CSPs (red) onto the tandem RRM1,2 structure. (**B**) ITC data shown for the binding of “CN--GG” RNA to $Npl3^{120\text{-}280}$-RRM1 (left), $Npl3^{120\text{-}280}$-linker (middle) and $Npl3^{120\text{-}280}$-RRM2 (right), respectively. (**C**) ITC data shown for binding of “CN--AA” RNA with $Npl3^{120\text{-}280}$ (left) and $Npl3^{120\text{-}280}$-linker (middle). K_D calculated from NMR titrations (right panel) upon addition of ”CN—AA” RNA to $npl3^{120\text{-}280}$ (see Supplementary Figure S6A).

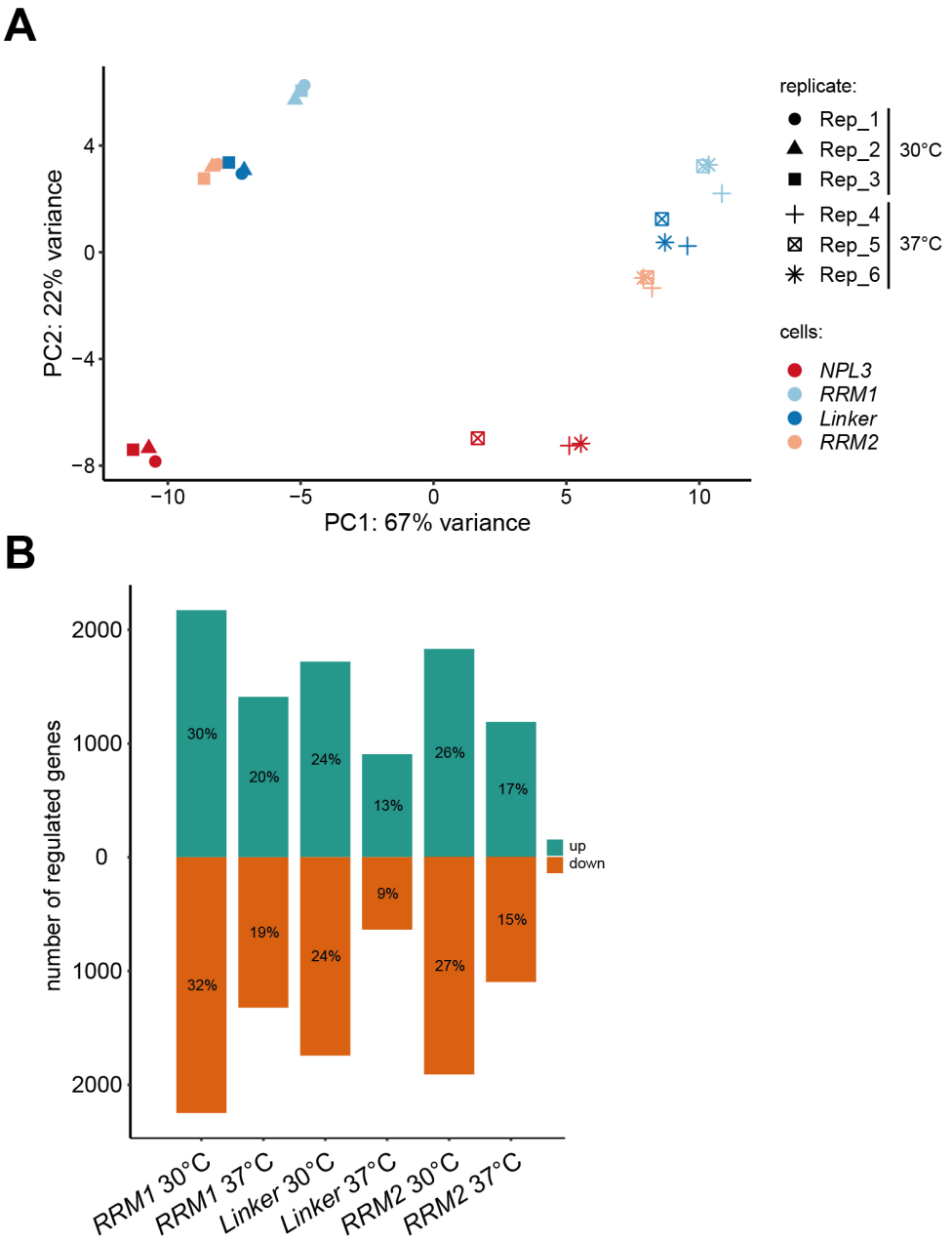

Supplementary Figure S9. Mutations in *NPL3* lead to substantial changes in transcript abundance. (**A**) Principle component analysis of regularized-logarithm transformed RNA-seq read counts based on 500 most variable genes across all samples. Scatter plot shows the first two principle components (PC1 and PC2) to evaluate the variance between wt and *npl3* mutants at 30°C and 37°C. Each condition comprises three biological replicates. (**B**) Hundreds of transcripts change in abundance in the *npl3* mutants. Bar diagram depicts number and percentages of significantly up-regulated (green) and down-regulated (orange) genes (adjusted p-value < 0.05) in the three *npl3* mutants at 30°C and 37°C.

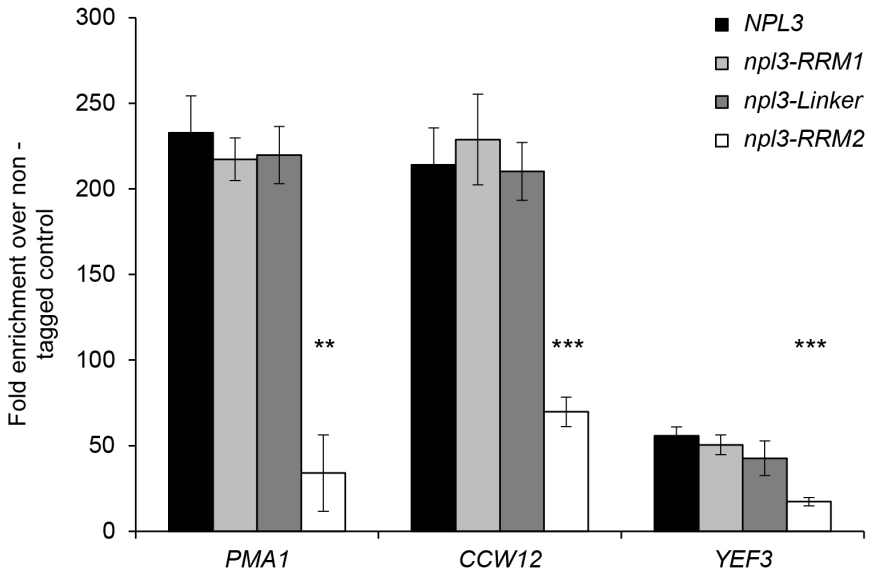

Supplementary Figure S10. RNA binding of the CBC subunit Cbc2 is not reduced in *npl3-RRM1* and *-Linker* cells *in vivo*. TAP-tagged Cbc2 was immunoprecipitated from whole-cell extracts of *NPL3*, *npl3-RRM1*, *-Linker* and *-RRM2* cells. The amount of co-immunoprecipitated RNA was quantified by RT-qPCR for the indicated transcripts. The amount of co-immunoprecipitated mRNA was calculated as the enrichment over the amount of RNA in a control experiment with a strain expressing non-tagged Cbc2.

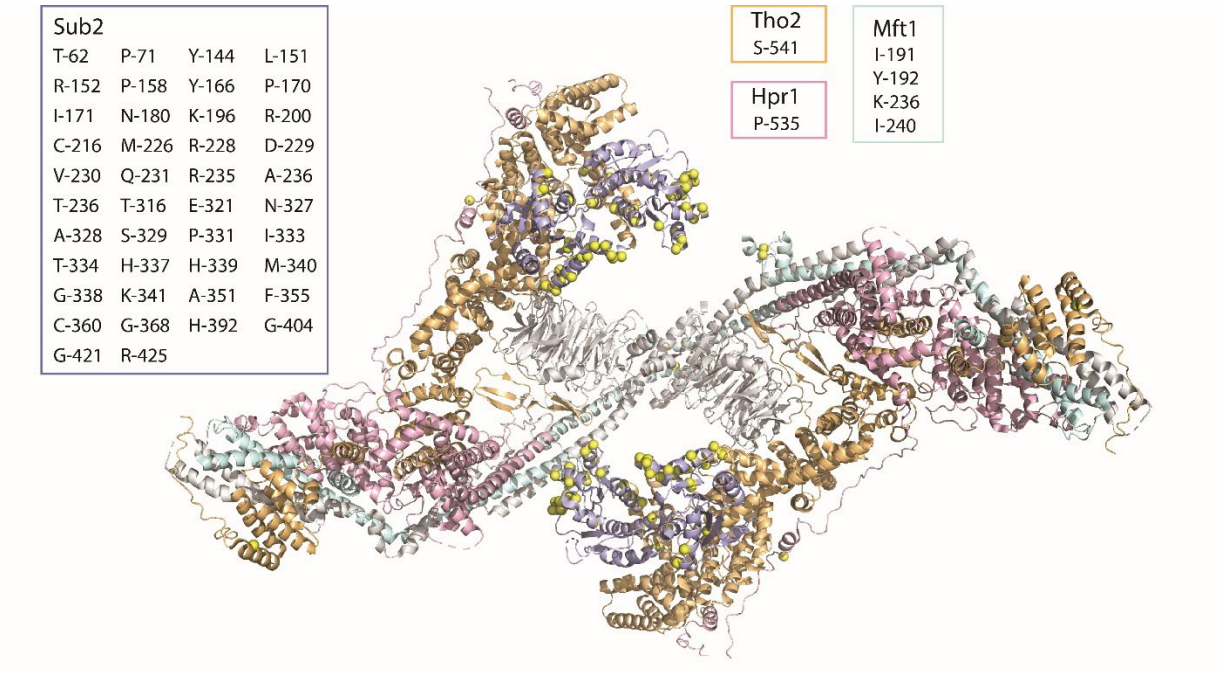

Supplementary Figure S11. 3D structure of THO-Sub2 complex (3) with RNA crosslinking sites in Tho2, Hpr1, Mft1 and Sub2 (Supplementary Table S1 and S2). Amino acids crosslinked to RNA are depicted as yellow spheres. Coloring scheme of the proteins with crosslinking sites is illustrated. The crosslinking sites of the respective proteins are listed within the inlets.

Supplementary Table S1. Amino Acids identified to be cross-linked to RNA *in vivo* by RNP^{XL}
Protein names with asterisk indicate those peptides with their crosslinked amino acids that have been previously identified (4). Asterisks in parentheses mark the crosslinked amino acids identified in this study.

Protein	Cross-linked peptide	Cross-linked amino acid	Source
Npl3	127-LFVRPFPLDVQESELNEIFGPFGPMK-152	127-152	Cbc2
Npl3*	156-ILNGFAFVEFEEAESAAK-173	F160 or F162 or F165	Cbc2
Npl3*	182-SFANQPLEVVYSKLP(*)AK-198	P196	Hpr1, Sub2, Cbc2, Npl3, Mtr2, oligo(dT)
Npl3*	222-ENSLETTFSSVNTR-235	F229 or S230 and R235	Cbc2, Hpr1, Mtr2, Npl3
Npl3	273-DDNPPP(*)IR-280	P278	Cbc2, Npl3
Npl3	273-DDNPPPIR(*)R-281	R280	Sub2, Hpr1, Tho1, Cbc2, Mtr2, Nab2, Npl3
Npl3	371-NDYGP(*)PR-377	P375	Hpr1, Cbc2
Npl3	392-GDYG(*)P(*)PR-398	G395 and P396	Cbc2, Hpr1
Npl3	385-GGYDGPRGDYGPPRDAYR(*)TR-404	R402	Sub2
Sto1	7-RGDF(*)DEDENYR-17	R7	Cbc2
Sto1	18-DF(*)RPR-22	F19	Cbc2
Sto1	18-DFRP(*)R-22	P21	Cbc2
Sto1	107-NNVAGKSIINYFFEELQK-124	K112 or S113	Thp1
Sto1	578-K(*)NDLYFR-584	K578	Cbc2
Cbc2	17-RL(*)DTPSR-23	L18	Cbc2
Cbc2	31-R(*)NPNGLQELR-40	R31	Sub2, Cbc2
Cbc2	134-GK(*)SGGQVSDELR-145	K135	Cbc2
Cbc2	146-FDFDASRGGFAIPFAER-162	146-162	Cbc2
Cbc2	163-VGVP(*)HSR-169	P166	Cbc2
Tho2	1183-LPSSALIGH(*)LK-1193	H1191	Hpr1
Tho2	1357-TLIQNPQNP(*)DFAEK-1370	P1365	Hpr1, Sub2
Hpr1	534-IP(*)TGLDK-540	P535	Thp1
Mft1	189-YRIYDDFSK-197	I191 or Y192	Hpr1, Sub2
Gbp2	98-GR(*)TLGPIVER-107	R-99 and G-98 or G-102	Hpr1, Sub2
Gbp2	100-TLGP(*)IVER-107	P-103	Sub2
Hrb1	51-FADTY(*)RGSR-59	Y55	Hpr1
Hrb1	137-GDYGP(*)LLAR-145	P141	Hpr1, Sub2
Hrb1	190-ADIITSRGHHR-200	S195 or R196	Hpr1, Cbc2, Mtr2
Sub2	53-K(*)GSYVGIHSTGFK-65	K53	Sub2
Sub2	53-KG(*)SY(*)VGIHSTGFK-65	G54 and Y56	Sub2
Sub2	54-GSYVGIHST(*)GFKDFLLKPELSR-75	T62	Sub2
Sub2	66-DFLLKP(*)ELSR-75	K70	Sub2
Sub2	141-ELAY(*)QIR-147	Y144	Sub2
Sub2*	162-TAVFYGGTP(*)ISK-173	P170	Sub2, Hpr1, oligo(dT)

Sub2	180-NKDTAPHIVVATPGR-194	N180 or K181	Sub2
Sub2	195-LK(*)ALVR-200	K196	Sub2
Sub2	197-ALVR(*)EK-202	R200	Hpr1, Mtr2
Sub2	201-EKYIDLSHVK-210	E201 or K202	Sub2
Sub2	203-Y(*)IDLSHVK-210	Y203	Sub2
Sub2	211-NFVIDEC(*)DK-219	C217	Sub2
Sub2	228-RDVQEIFR-235	R228 or D229	Sub2
Sub2	228-RDVQEIFR(*)ATPR-239	R235	Sub2
Sub2	260-RF(*)LQNPLEIFVDDEAK-275	F261	Sub2
Sub2	315-STTRANELTK-324	T316 or T317	Hpr1, Mtr2
Sub2*	325-LLNASNFPAITVHGH(*)MK-341	H339	Sub2, oligo(dT), Hpr1
Sub2	351-AFKDF(*)EK-357	F355	Sub2
Sub2	359-IC(*)VSTDVFGR-368	C360	Sub2
Sub2	369-G(*)IDIER-374	G369	Sub2
Sub2	375-INLAINYDLTNEADQYLH(*)R-393	H392	Sub2
Sub2	404-G(*)LAISFVSSK-413	G404	Sub2
Sub2	414-EDEEVLAK(*)IQER-425	K421	Sub2
Yra1	8-SLDEIIG(*)SNKAGSNR-22	G14 and K17 or A18	Sub2
Yra1	8-SLDEIIGSNKAG(*)SNR-22	G19	Sub2, Hpr1, Mtr2
Yra1	25-V(*)G(*)G(*)T(*)R(*)GNGPR-34	25-29	Mtr2, Hpr1, Tho1, Cbc2
Yra1	36-VG(*)K(*)QVGSQR-44	G37 and K38	Cbc2, Mtr2, Hpr1, Nab2
Yra1	45-R(*)S(*)LP(*)NR-50	R45, S46 and P48	Hpr1, Tho1, Cbc2, Mtr2, Nab2
Yra1	51-R(*)GP(*)IR-55	R51 and P53	Sub2, Hpr1, Tho1, Mtr2, Cbc2, Nab2, Npl3
Yra1	57-NTR(*)APPNAVAR-67	R59	Sub2, Tho1, Cbc2, Mtr2
Yra1*	57-NTRAP(*)PNAVAR-67	P61	oligo(dT), Tho1, Hpr1, Mtr2, Nab2, Npl3
Yra1	57-NTRAPP(*)NAVAR-67	P62	Hpr1, Cbc2, Mtr2, Nab2
Yra1	60-APPNAVAR(*)VAK-70	R67	Sub2, Nab2, Mtr2
Yra1	68-VAK(*)LLDTTR-76	K70	Hpr1, Sub2, Mtr2
Yra1	80-VNVEGLPRDIK-90	P86 or R87	Hpr1, Sub2
Yra1	108-VLLSYNER(*)GQSTGMANITFK-127	R115	Sub2
Yra1	139-FNGSPIDGGRSR-150	146-GGRSR-150	Sub2, Hpr1, Mtr2, Nab2, Npl3
Yra1*	153-LNLIVDP(*)NQR(*)PVK-165	P159 and R162	Hpr1, Sub2, oligo(dT)
Yra1*	153-LNLIVDPNQRP(*)VK-165	P163	Sub2, Mtr2, oligo(dT)
Yra1	178-GGNAP(*)R(*)P(*)VK-186	P182, R183 and P184	Hpr1, Tho1, Cbc2, Nab2, Mtr2
Yra1	210-KSLEDLDK-217	K210 or S211	Sub2
Yra2	38-LGFAPSDAASR(*)SK-50	R48	Cbc2
Tho1	75-KEVSSEPK-82	75-82	Nab2
Tho1	129-ALDLLNK(*)K-136	K135	Tho1
Tho1	140-ANKF(*)GQDQADIDSLQR-155	F143	Tho1
Tho1	181-KNEPESGNNGKFK-193	G190 or K191 or F192	Tho1

Tho1	214-SGYRR-218	G215 or Y216 or R217	Tho1
Nab2	210-GGGAVGK(*)NR-218	K216	Nab2
Nab2	314-TREEFQK-320	314-320	Nab2
Nab2	322-KADL(*)LAAK-329	L325	Nab2
Nab2	322-KADLLAAK(*)R-330	K329	Nab2
Nab2	394-EVKPISQK(*)K-402	K401	Nab2
Nab2	403-AAPPP(*)VEK-410	P407	Nab2
Nab2	411-SLEQC(*)K-416	C415	Nab2
Nab2	417-FGTHC(*)TNK-424	C421	Nab2
Nab2	433-SHIMC(*)R-438	C437	Nab2
Sac3	460-ALSH(*)TLNK-467	H463	Thp1
Sac3	527-TYLTC(*)LER-534	C531	Thp1
Sac3	862-NLIFSPVNDEFNK(*)FATHLTK-881	K874	Thp1
Sac3	1084-YDK(*)TLR-1089	K1086	Thp1
Sac3	1116-KMLEKEK(*)-1122	K1122	Nab2
Cdc31	51-ALGFELP(*)KR-59	P57	Thp1
Cdc31	113-ISIK(*)NLR-119	K116	Thp1
Cdc31	121-VAK(*)ELGETLTDEELR-135	K123	Thp1
Mex67	428-YNH(*)GYNSTSNNK-439	H430	Mtr2
Mtr2	102-VR(*)FDESGR-109	R-103	Mtr2
Mtr2	38-LAQFVQLFNPNNCR-51	C-50	Mtr2
Pab1*	307-QYEAYRLEK-315	Y308 and Y311	Cbc2, Npl3, Nab2
Cbf5	467-KSEDGDSEEKK-477	S-468 or S-473	Cbc2
Cbf5	420-EVETE(*)KEEVK-42	E-424	Sub2
Msl5	90-KNRSPSPPPVY(*)DAQGK-105	Y-100	Tho1
Msl5	268-E(*)DNRPCPICGLKDHK-282	E-268	Sub2
Nam8	237-VGPTSGQQQH(*)VSGNNDYNR-25	H-246 and Q-245 or Q-244 or Q-243	Cbc2
Prp19	140-SSQQAV(*)AITR-149	V-145	Mtr2
Yhc1	44-DIINKHNHK-52	N-47 or N-50	Cbc22
Yhc1	55-HIGKRGR-61	H-55	Hpr1

Supplementary Table S2. Identified crosslinks of TREX components
Index numbers indicate the MS2 spectrum identified in the respective idXml file of the affinity purifications. See Excel table.

Supplementary Table S3. Crosslinks identified by a database search against the entire yeast database
Index numbers list the MS2 spectra of crosslinks in the respective Affinity purification with their respective idXml files. See Excel table.

Supplementary Table S4A. List of oligonucleotides used NMR binding studies

	Npl3 domains	oligo	NMR CSP[b]	Binding[c]
DNA oligonucleotides (single stranded)[a]	RRM1	TTTTT	0.01	no
		GGGGG	0.05	no
		AAA AA	0.01	no
		CCCCC	0.44	yes
		AGCCCC	0.31	yes
		AGCACC	0.08	yes
	RRM2	TTTTT	0.11	yes
		CCCCC	0.00	no
		AAA AA	0.01	no
		GGGGG	0.08	yes
		GGGGAGA	0.05	no
		GTGGGGA	0.06	no
		GTGGAGA	0.41	yes
		GTAAAGA	0.11	yes
	RRM1,2	AGCACCGTGGAGA	0.34	yes

[a] DNA oligos were used as proxy for RNA
[b] Maximal NMR chemical shift perturbation observed at 4-fold excess of the oligonucleotide
[c] Above a CSP threshold ≤ 0.08

Supplementary Table S4B. Isothermal titration calorimetry (ITC) and NMR binding assays for the protein-RNA interactions

Protein	RNA	K_D (μM)	N	ΔH(kJ/mol)	TΔS (kJ/mol)	ΔG (kJ/mol)
$Npl3^{120-280}$	CN--GG	0.66 ± 0.04	0.9	-67.5 ± 0.8	-32.2	-35.3
$npl3^{120-280}$-Linker	CN--GG	Not detected	-	-	-	-
$npl3^{120-280}$-RRM1	CN--GG	10.4 ± 2	0.97	-127 ± 15.6	-98.2	-28.5
$npl3^{120-280}$-RRM2	CN--GG	4.8 ± 0.3	1.08	-118 ± 3.2	-87.8	-30.4
$Npl3^{120-280}$	CN--AA	Not detected	-	-	-	-
$npl3^{120-280}$-Linker	CN--AA	Not detected	-	-	-	-
$Npl3^{120-280}$	CN--AA	143 ± 25 (by NMR)	-	-	-	-

Supplementary Table S5. Small angle X-ray scattering of free and RNA bound RRM1,2 of Npl3

Sample	R_g (Angstrom)	D_{max} (Angstrom)
$Npl3^{120-280}$	20.4 ± 0.12	67.7
$Npl3^{120-280}$ + CN--GG	20.4 ± 0.16	63.6

npl3$^{120-280}$-Linker	19.0 ± 0.10	66.5

Supplementary Table S6. Structural statistics

Npl3$^{120-280}$ RRM1,2 free form	**Statistics**
Intra-domain PRE restraints	69
Inter-domain PRE restraints	31
Distance violations	4 (<3 Å)
Average RMSD for 15 lowest energy structures[a]	0.93 Å
PRE quality factor[b]	0.10
Agreement with SAXS data (χ^2)	2.70
Backbone structural quality (Ramachandran plot)	82.8% (allowed) 14.8% (additionally allowed), 1.6 % (generously allowed) 0.8% (dis-allowed)

[a] out of 100 structures calculated
[b] see methods

Supplementary Table S7. Differential expression analysis using DESeq2

See Excel table.

Supplementary Table S8. Quantitative MS proteomic data of the Cbc2-TAP purifications from *npl3-Linker* and wt cells.

See Excel table.

Supplementary Table S9. Yeast Strains

Yeast Strain	**Genotype**	**Reference**
RS453	MAT a, ade2-1, his3-11,15, ura3-52, leu2-3,112, trp1-1, can1-100, GAL+	Sträßer K. 2000
SUB2-TAP	MAT a, ade2-1, his3-11,15, ura3-52, leu2-3,112, trp1-1, can1-100, GAL+, SUB2-CBP-TEV-2x protA::TRP1-KL	Sträßer K. 2002
HPR1-FTpA	MAT a, ade2-1, his3-11,15, ura3-52, leu2-3,112, trp1-1, can1-100, GAL+, HPR1-FLAG-TEV-2x protA::HIS3MX4	This study
TAP-NPL3	MAT a, ade2-1, his3-11,15, ura3-52, leu2-3,112, trp1-1, can1-100, GAL+, 2x protA-TEV-NPL3::TRP1-KL	This study
THO1-FTpA	MAT a, ade2-1, his3-11,15, ura3-52, leu2-3,112, trp1-1, can1-100, GAL+, THO1-FLAG-TEV-2x protA::HIS3MX4	This study
NAB2-FTpA	MAT a, ade2-1, his3-11,15, ura3-52, leu2-3,112, trp1-1, can1-100, GAL+, NAB2-FLAG-TEV-2x protA::HISMX4	This study
MTR2-FTpA	MAT a, ade2-1, his3-11,15, ura3-52, leu2-3,112, trp1-1, can1-100, GAL+, MTR2-FLAG-TEV-2x protA::HIS3MX4	This study
CBC2-FTpA	MAT a, ade2-1, his3-11,15, ura3-52, leu2-3,112, trp1-1, can1-100, GAL+, CBC2-FLAG-TEV-2x protA::HIS3MX4	This study
THP1-TAP	MAT a, ade2-1, his3-11,15, ura3-52, leu2-3,112, trp1-1, can1-100, GAL+, THP1-CBP-TEV-2x protA::TRP1-KL	This study
W303	MATa, ura3-1, trp1-1, his3-11,15, leu2-3,112, ade2-1, can1-100 GAL+	Thomas B.J. 1989

npl3 shuffle	MATa, ura3-1, trp1-1, his3-11,15, leu2-3,112, ade2-1, can1-100 GAL+, NPL3::HIS3, pRS316-NPL3	This study
npl3 shuffle *CBC2-TAP*	MATa, ura3-1, trp1-1, his3-11,15, leu2-3,112, ade2-1, can1-100 GAL+, NPL3::HIS3, pRS316-NPL3, CBC2-CBP-TEV-2x protA::TRP1-KL	This study
npl3 shuffle *CBC2-TAP MEX67-HA*	MATa, ura3-1, trp1-1, his3-11,15, leu2-3,112, ade2-1, can1-100 GAL+, NPL3::HIS3, pRS316-NPL3, CBC2-CBP-TEV-2x protA::TRP1-KL, MEX67-HA::KanMX4	This study
npl3 shuffle *CBC2-TAP HPR1-HA*	MATa, ura3-1, trp1-1, his3-11,15, leu2-3,112, ade2-1, can1-100 GAL+, NPL3::HIS3, pRS316-NPL3, CBC2-CBP-TEV-2x protA::TRP1-KL, HPR1-HA::KanMX4	This study
npl3 shuffle *MEX67-HA*	MATa, ura3-1, trp1-1, his3-11,15, leu2-3,112, ade2-1, can1-100 GAL+, NPL3::HIS3, pRS316-NPL3, MEX67-HA::KanMX4	This study
npl3 shuffle *HPR1-HA*	MATa, ura3-1, trp1-1, his3-11,15, leu2-3,112, ade2-1, can1-100 GAL+, NPL3::HIS3, pRS316-NPL3, HPR1-HA::KanMX4	This study
npl3 shuffle *SUB2-FTpA*	MATa, ura3-1, trp1-1, his3-11,15, leu2-3,112, ade2-1, can1-100 GAL+, NPL3::HIS3, pRS316-NPL3	This study
npl3 shuffle THO1-FTpA	MATa, ura3-1, trp1-1, his3-11,15, leu2-3,112, ade2-1, can1-100 GAL+, NPL3::HIS3, pRS316-NPL3	This study
npl3 shuffle *MEX67-FTpA*	MATa, ura3-1, trp1-1, his3-11,15, leu2-3,112, ade2-1, can1-100 GAL+, NPL3::HIS3, pRS316-NPL3	This study
npl3 shuffle *HPR1-FTpA*	MATa, ura3-1, trp1-1, his3-11,15, leu2-3,112, ade2-1, can1-100 GAL+, NPL3::HIS3, pRS316-NPL3	This study

Supplementary Table S10. Plasmids

Plasmid	Description	Reference
pBS1479	For genomic C-terminal TAP-tagging (CBP-TEV-2x protein A), *TRP1-KL*	Puig O. 2001
pFA6a-FTpA-HIS3MX4	For genomic C-terminal FTpA-tagging (FLAG-TEV-2x protein A), *HIS3MX4*	Kressler D. 2012
pRS316-*NPL3*	pBlueScript based yeast centromere vector with *URA3* marker and ORF + 500 bp of 5' and 300 bp of 3' UTR of *NPL3*	This study
pRS315	pBlueScript based yeast centromere vector with *LEU2* marker	Sikorski R.S. 1989
pRS315-*NPL3*	ORF + 500 bp of 5' and 300 bp of 3' UTR of *NPL3* was cloned into pRS315	This study
pRS315-*npl3-F160Y,F162Y,F165Y*	*npl3-F160Y,F162Y,F165Y*	This study
pRS315-*npl3-F160Y,F162Y*	*npl3-F160Y,F162Y*	This study
pRS315-*npl3-F160Y,F165Y*	*npl3-F160Y,F165Y*	This study
pRS315-*npl3-F162Y,F165Y*	*npl3-F162Y,F165Y*	This study
pRS315-*npl3- F160Y*	*npl3-F160Y*	This study
pRS315-*npl3-F162Y (RRM1)*	*npl3-F162Y (RRM1)*	This study
pRS315-*npl3- F165Y*	*npl3-F165Y*	This study
pRS315-*npl3-P196D,A197D (Linker)*	*npl3-P196D,A197D (Linker)*	This study
pRS315-*npl3-F245I (RRM2)*	*npl3-F245I (RRM2)*	This study
pRS315-*npl3-F245Y*	*npl3-F245Y*	This study

pRS315-*npl3-RRM1-Linker*	*npl3-F162Y,P196D,A197D*	This study
pRS315-*npl3-RRM1-RRM2*	*npl3-F162Y,F245I*	This study
pRS315-*npl3-Linker-RRM2*	*npl3-P196D,A197D,F245I*	This study
pRS315-*npl3-RRM1-Linker-RRM2*	*npl3-F162Y,P196D,A197D,F245I*	This study
pRS315-*TAP-NPL3*	*2x prot A-TEV-CBP-NPL3*	This study
pRS315-*TAP-npl3-RRM1*	*2x prot A-TEV-CBP-npl3-F162Y*	This study
pRS315-*TAP-npl3-Linker*	*2x prot A-TEV-CBP-npl3-P196D,A197D*	This study
pRS315-*TAP-npl3-F245I (RRM2)*	*2x prot A-TEV-CBP-*n*pl3-F245I*	This study
pRS315-*TAP-npl3-F245Y*	*2x prot A-TEV-CBP-*n*pl3-F245Y*	This study
pRS315-*TAP-npl3-RRM1-Linker*	*2x prot A-TEV-CBP-npl3-F162Y,P196D,A197D*	This study
pRS315-TAP-*npl3-RRM1-RRM2*	*2x prot A-TEV-CBP-npl3-F162Y,F245I*	This study
pRS315-TAP-*npl3-Linker-RRM2*	*2x prot A-TEV-CBP-npl3-P196D,A197D,F245I*	This study
pRS315-TAP-*npl3-RRM1-Linker-RRM2*	*2x prot A-TEV-CBP-npl3-F162Y,P196D,A197D,F245I*	This study
pRS425	*high copy number plasmid, 2µ, with LEU2 maker*	(5)
pRS425-*NPL3*	*ORF + 500 bp of 5' and 300 bp of 3' UTR of NPL3 was cloned into pRS425*	This study
pRS425-*npl3-RRM1*	*npl3-F162Y (RRM1)*	This study
pRS425-*npl3-Linker*	*npl3-P196D,A197D (Linker)*	This study
pRS425-*npl3-RRM2*	*npl3-F245I (RRM2)*	This study
pYM14	For genomic C-terminal HA-tagging, KanMX4	Janke C., 2004
pT7-His6-TEV-NPL3 (RRMs, 121-280)	For recombinant expression of both RRM domains of Npl3; His6-TEV-Npl3 (aa121-aa280)	This study
pT7-His6-TEV-*npl3-RRM1* (RRMs, 121-280)	For recombinant expression of both RRM domains of npl3-RRM1	This study
pT7-His6-TEV-*npl3-Linker* (RRMs, 121-280)	For recombinant expression of both RRM domains of npl3-Linker	This study
pT7-His6-TEV-*npl3-RRM2* (RRMs, 121-280)	For recombinant expression of both RRM domains of npl3-RRM2	This study
pT7-His6-TEV-NPL3 (RRMs, 120-280)	Recombinant expression and purification of Npl3-RRM1,2 for NMR experiments	This study
pT7-His6-TEV-NPL3-RRM1 only	Recombinant expression and purification of Npl3-RRM1 for NMR titration experiments	This study
pT7-His6-TEV-NPL3-RRM2 only	Recombinant expression and purification of Npl3-RRM2 for NMR titration experiments	This study
npl3-D135C & C211S	Single cysteine mutant D135C of Npl3-RRM1,2 for PRE experiments	This study
npl3-E176C & C211S	Single cysteine mutant E176C of Npl3-RRM1,2 for PRE experiments	This study
npl3-N185C & C211S	Single cysteine mutant N185C of Npl3-RRM1,2 for PRE experiments	This study

npl3-D236C & C211S	Single cysteine mutant D236C of Npl3-RRM1,2 for PRE experiments	This study

Supplementary Table S11. Primers

Primers used for genomic tagging	Sequence (5' to 3')
HPR1-FTpA fwd	GCAGCTACTTCGAACATTTCTAATGGTTCATCTACCCAAGATATGAAAGATCACGACGGTGACTAC
HPR1-FTpA rev	TGCATGAATTTCTTATCAGTTTAAAATTTCTATTAAGAGGATAATTTAATCGATGAATTCGAGCTCG
THO1-FTpA fwd	TCCAGAGTAAGTAAAAACAGGAGAGGCAACCGCTCTGGTTACAGAAGAGATCACGACGGTGACTAC
THO1-FTpA rev	GAACCGAAACTAGAATGAAAAACTCCACCAAAACGGCTTGAGCCTTTAATCGATGAATTCGAGCTCG
NAB2-FTpA fwd	CCTCCGCAAACCAGTTTTACGCACCAAGAACAAGATACGGAAATGAACGATCACGACGGTGACTAC
NAB2-FTpA rev	AAGGGTCACAGGAACATGAATTTCGTTCCGTGATTTTAATAGTAATCAATCGATGAATTCGAGCTCG
MTR2-FTpA fwd	TTTAACTATAACATGGTTTACAAACCCGAGGATTCTCTGCTAAAAATTGATCACGACGGTGACTAC
MTR2-FTpA rev	TTTCTATATAATTTTGTTTTTCCCTGGTAGAGCGGAATCTTCCCACTAATCGATGAATTCGAGCTCG
CBC2-FTpA fwd	AGACCAGGTTTCGATGAAGAAAGAGAAGATGATAACTACGTACCTCAGGATCACGACGGTGACTAC
CBC2-FTpA rev	ATATATCTGTGTGTAGAATCTTTCTCAGATATAAATTGATTGATTCTAATCGATGAATTCGAGCTCG
THP1-FTpA fwd	AATGAACGAATCACCAAGATGTTTCCTGCCCATTCTCACGTTCTTTGGGATCACGACGGTGACTAC
THP1-FTpA rev	TGATATGTAGATATATATAGGAAATAGAAGAGAAGGAGCGACATTATGATCGATGAA TTCGAGCTCG
CBC2-TAP fw	AGACCAGGTTTCGATGAAGAAAGAGAAGATGATAACTACGTACCTCAGTCCATGGAAAAGAGAAG
CBC2-TAP rev	TATATATATCTGTGTGTAGAATCTTTCTCAGATATAAATTGATTGATTCTATACGACTCACTATAGGG
MEX67-HA fwd	TAAACTGTATATTTTTTGTGATACTGTGCGGCTGAAACAGGGAACAATATCATTAATCGATGAATTCGAGCTCG
MEX67-HA rev	AAAGGGTTTTCAGAGTAGCATGAATGGCATCCCTAGAGAAGCATTTGTGCAGTTCCGTACGCTGCAGGTCGAC
HPR1-HA fwd	GCTACTTCGAACATTTCTAATGGTTCATCTACCCAAGATATGAAACGTACGCTGCAGGTCGAC
HPR1-HA rev	ATGAATTTCTTATCAGTTTAAAATTTCTATTAAGAGGATAATTTAATCGATGAA TTCGAGCTCG
SUB2-FTpA fwd	GCTGAATTCCCAGAAGAAGGCATTGATCCGTCCACTTATTTGAATAATGATCACGACGGTGACTAC
SUB2-FTpA rev	AAAATCTTTATATAATCTATATAAAAACGTATCTTTTTTCCTTTATTAATCGATGAATTCGAGCTCG
MEX67-FTpA fwd	TTTCAGAGTAGCATGAATGGCATCCCTAGAGAAGCATTTGTGCAGTTCGATCACGACGGTGACTAC
MEX67-FTpA rev	TATATTTTTTGTGATACTGTGCGGCTGAAACAGGGAACAATATCATTAATCGATGAATTCGAGCTCG

REFERENCES

1. Simon, B., Madl, T., Mackereth, C.D., Nilges, M. and Sattler, M. (2010) An efficient protocol for NMR-spectroscopy-based structure determination of protein complexes in solution. *Angewandte Chemie*, **49**, 1967-1970.
2. Clery, A., Krepl, M., Nguyen, C.K.X., Moursy, A., Jorjani, H., Katsantoni, M., Okoniewski, M., Mittal, N., Zavolan, M., Sponer, J. *et al.* (2021) Structure of SRSF1 RRM1 bound to RNA reveals an unexpected bimodal mode of interaction and explains its involvement in SMN1 exon7 splicing. *Nat Commun*, **12**, 428.
3. Schuller, S.K., Schuller, J.M., Prabu, J.R., Baumgartner, M., Bonneau, F., Basquin, J. and Conti, E. (2020) Structural insights into the nucleic acid remodeling mechanisms of the yeast THO-Sub2 complex. *eLife*, **9**.
4. Kramer, K., Sachsenberg, T., Beckmann, B.M., Qamar, S., Boon, K.L., Hentze, M.W., Kohlbacher, O. and Urlaub, H. (2014) Photo-cross-linking and high-resolution mass spectrometry for assignment of RNA-binding sites in RNA-binding proteins. *Nat Methods*, **11**, 1064-1070.
5. Sikorski, R.S. and Hieter, P. (1989) A system of shuttle vectors and yeast host strains designed for efficient manipulation of DNA in Saccharomyces cerevisiae. *Genetics*, **122**, 19-27.